Electronic Supplementary Material (ESI) for Nanoscale.

Supplementary information

Induced Spin Polarization in Graphene via Interaction with Halogen Doped MoS_2 and $MoSe_2$ Monolayers by DFT Calculations

Ekaterina V. Sukhanova, [a,b] *Dmitry. G. Kvashnin* [a,b] *and Zakhar I. Popov* [b,c]

[a]Moscow Institute of Physics and Technology (State University), 9 Institutskiy per., Dolgoprudny, Moscow Region, 141701, Russian Federation.

[b]Emanuel Institute of Biochemical Physics of RAS, 4 Kosygin Street, Moscow, 119334, Russian Federation.

[c]National University of Science and Technology MISiS, 4 Leninskiy prospekt, Moscow, 119049, Russian Federation.

SI1. Calculation details

1.1) Work function calculation

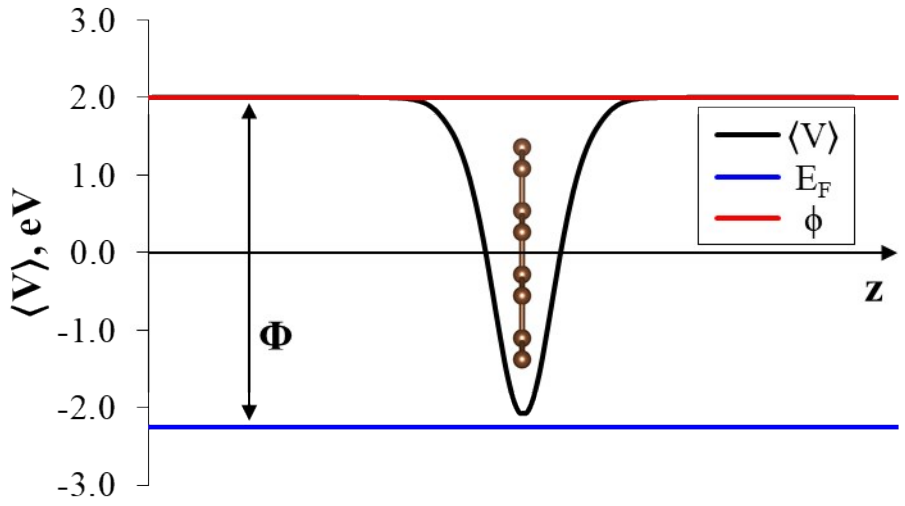

Figure S1. The averaged electrostatic potential $\langle V \rangle$ dependence on the z-direction for pristine graphene.

The work function (Φ) can be calculated as the difference between the vacuum level (ϕ) and the Fermi energy (E_F) of the system. The vacuum level (ϕ) can be found from the electrostatic potential averaged over (xy) plane dependence on the z coordinate. As an example, we presented the calculation of work function for pristine single-layer graphene:

$$\Phi = \phi - E_F = 2.00 - (-2.26) = 4.26 \text{ eV}$$

1.2) Charge density difference (CDD) analysis

In order to estimate the amount of charge transferred from graphene to MoX_2* (X = S, Se) layer the charge density difference analysis was carried out. The charge transfer can be determined as follow:

$$\Delta\rho(\vec{r}) = \rho_{Het}(\vec{r}) - \rho_{MoX_2^*}(\vec{r}) - \rho_{graphene}(\vec{r}),$$

where $\rho_{Het}(\vec{r})$, $\rho_{MoX_2^*}(\vec{r})$ and $\rho_{graphene}(\vec{r})$ are total charge densities of considered heterostructure, MoX_2* and graphene layers, respectively. The total amount of charge transfer can be estimated as:

$$\Delta Q(z) = \int_{-\infty}^{z} \Delta\rho(z')dz',$$

where $\Delta\rho(z')$ is the plane-averaged $\Delta\rho(\vec{r})$ among the normal direction to the heterostructure basal plane obtained by integration of $\Delta\rho(\vec{r})$ within the x-y plane at z' point. The number of charge transferred from graphene to MoX_2* (X = S, Se) layer can be estimated by finding the maximum (minimum) value of $\Delta Q(z)$.

1.3) Lattice mismatch calculation

The lattice mismatch in considered heterostructures was calculated as follow:

$$\alpha = \frac{\left|a_{graphene} - a_{MoX_2}\right|}{a_{graphene}} * 100\%,$$

where $a_{graphene}$ and a_{MoX_2} are the optimized lengths of graphene and MoX_2 supercells translation vectors, respectively.

The deformation of individual layers in heterostructures was calculated as:

$$\alpha = \frac{\left|a_{heterostructure} - a_{free}\right|}{a_{free}} * 100\%,$$

where $a_{heterostructure}$ and a_{free} are the structure translation vectors in heterostructure and individual layer, respectively.

SI2. Halogen-doped MoX_2 (X = S, Se) layers

The optimized lattice parameters of pristine graphene, MoS_2 and $MoSe_2$ layers are 2.468 Å, 3.164 Å and 3.293 Å, respectively. The obtained values are in a good agreement with experimental measurements[1,2].

1) The thermodynamics of defects formation in the MoX_2 structures

Chalcogen monovacancies formation for MoS_2 and $MoSe_2$ monolayers do not lead to the appearance of magnetic moment[3–8]. We used 4x4x1 and 3x3x1 supercells with one chalcogen atom vacancies in the case of MoS_2 and $MoSe_2$ monolayers, respectively. Such supercell size choice is due to future applications for the construction of heterostructures with graphene.

The monovacancies formation energies were calculated using the following equation:

$$E_f = E[MoX_2 vac] + E[X] - E[MoX_2\ pure],$$

where $E[MoX_2 vac]$ is the total energy of the defected MoX_2 layer with X atom vacancy, $E[X]$ is the chemical potential for X atom, $E[MoX_2\ pure]$ is the total energy of the pristine MoX_2 monolayer. The chemical potential of S atom was calculated from the bulk with Fddd space group, the unit cell of the crystal consists of 128 atoms. For Se atom chemical potential calculation a bulk crystal with $P3_121$ space group was used.

Calculated values of monovacancies formation energies are presented in Table S1.

Table S1. The chalcogen monovacancy formation energies for the MoX_2 (X = S, Se) structure.

	E_f, eV
S vacancy	2.70
Se vacancy	2.61

Obtained values of monovacancies formation energies are in a good agreement with previously reported values[4,6,9,10]. The positive value of monovacancies formation indicates that the process is endothermic, and the formation of defective structures is not energetically favorable.

Table S2. The binding energy of halogen atoms with MoX_2 structure

Dopant atom	MoS_2	$MoSe_2$
F	-2.96	-2.86
Cl	-1.51	-1.47
Br	-1.01	-0.96
I	-0.53	-0.47

2) Magnetic and electronic properties of defective MoX_2 structures

Table S3. The estimation of the atomic charges on the halogen dopant according to Bader charge analysis

Dopant atom	MoS_2	$MoSe_2$
F	-0.66 e	-0.68 e
Cl	-0.46 e	-0.52 e
Br	-0.33 e	-0.38 e
I	-0.14 e	-0.19 e

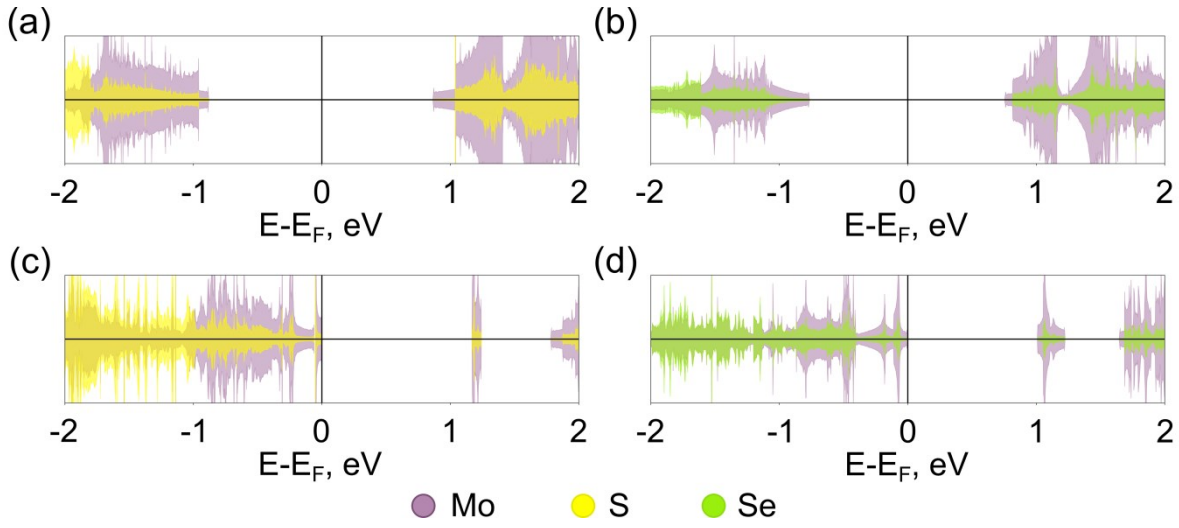

Figure S2. Atom and spin-resolved density of states for MoS_2 (a,c) and $MoSe_2$ (b,d) layers with perfect structure (a, b) and with monovacancy of chalcogen atom (c, d).

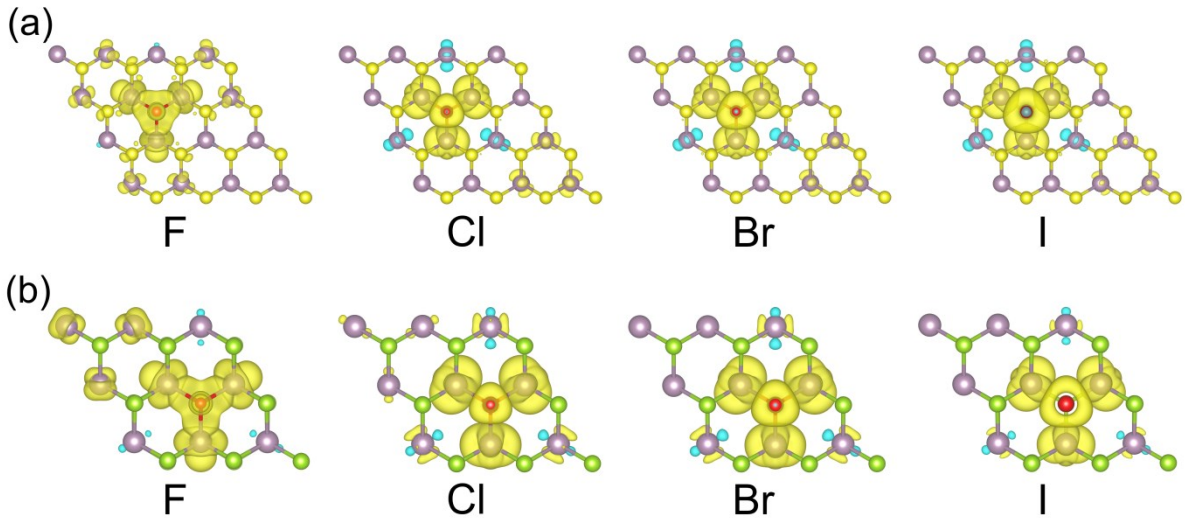

Figure S3. Spin density distribution in (a) MoS_2 and (b) $MoSe_2$ layers doped by halogen atoms (F, Cl, Br, I). By purple, yellow, green and red colors the Mo, S, Se and halogen atoms are depicted, respectively. By yellow and blue clouds electron distribution (the isosurface level is 10-3 e/Å3) with spin up and down is depicted.

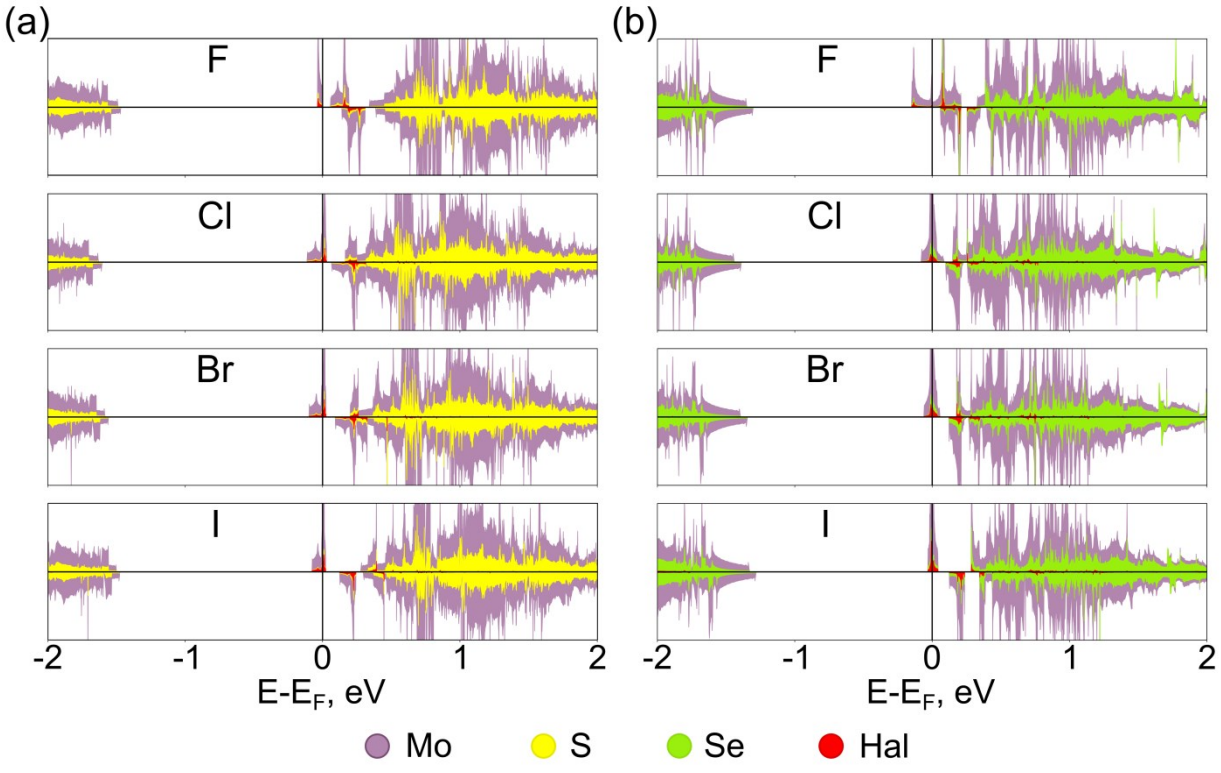

Figure S4. Spin and atom resolved DOS for MoS_2* and $MoSe_2$*. Purple, yellow, green and red lines corresponds to the electron density from Mo, S, Se and halogen (F, Cl, Br, I) atoms, respectively.

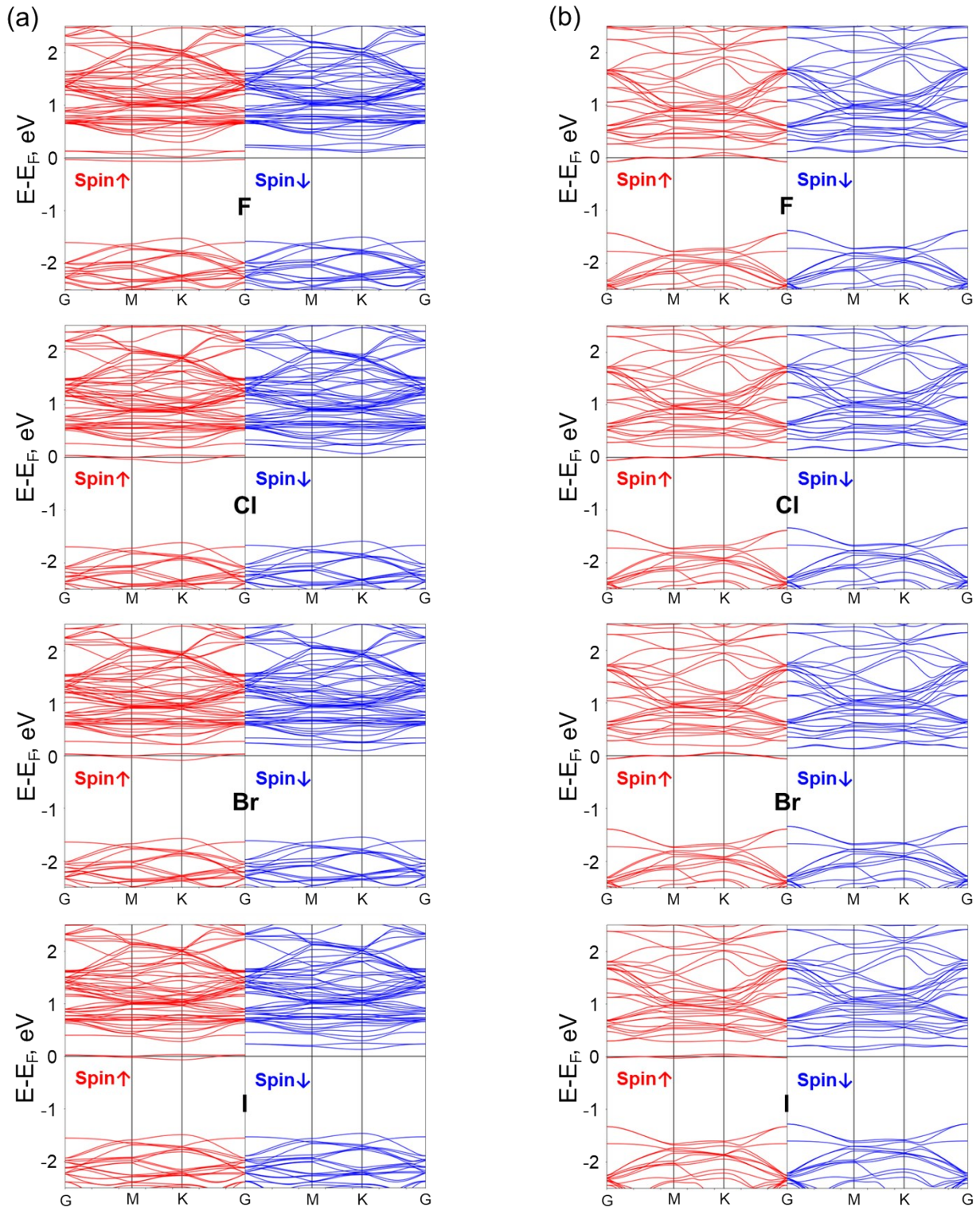

Figure S5. Spin-resolved electronic band structures for halogen doped (a) MoS_2 and (b) $MoSe_2$ monolayers.

SI3. MoX_2*/graphene heterostructures (X = S, Se; *= Ø, F, Cl, Br, I)

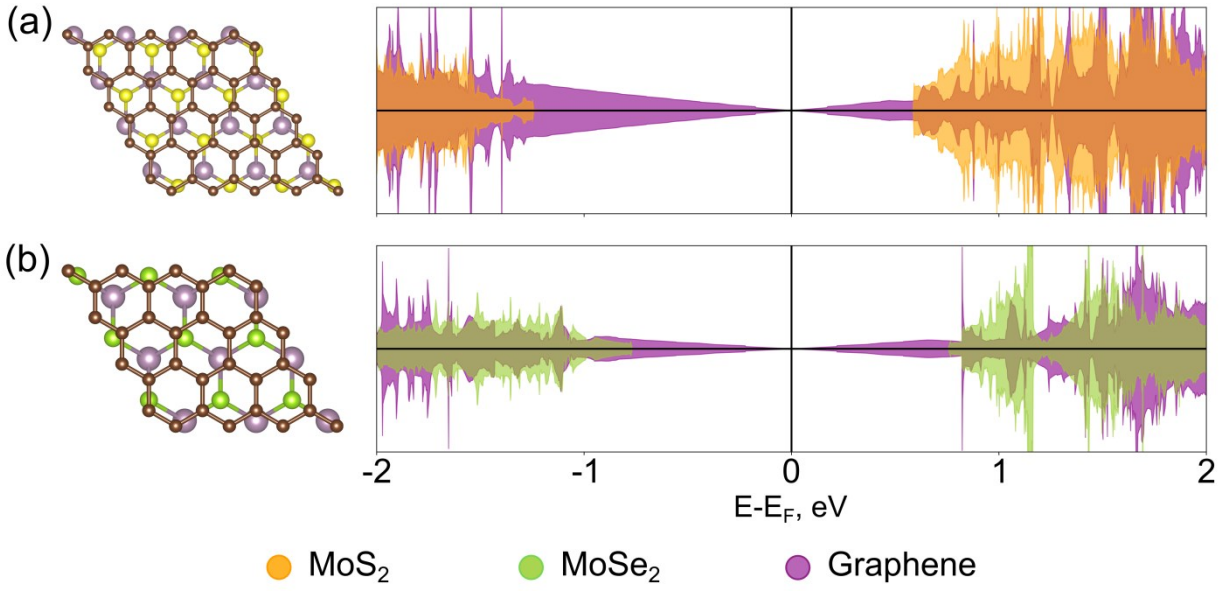

Figure S6. Atom-resolved density of states for pristine (a) MoS_2/graphene and (b) $MoSe_2$/graphene heterostructures. Contribution from graphene was enlarged by 10 times for better representation. It is worth mentioning that the Dirac cone is located in the vicinity of Fermi energy.

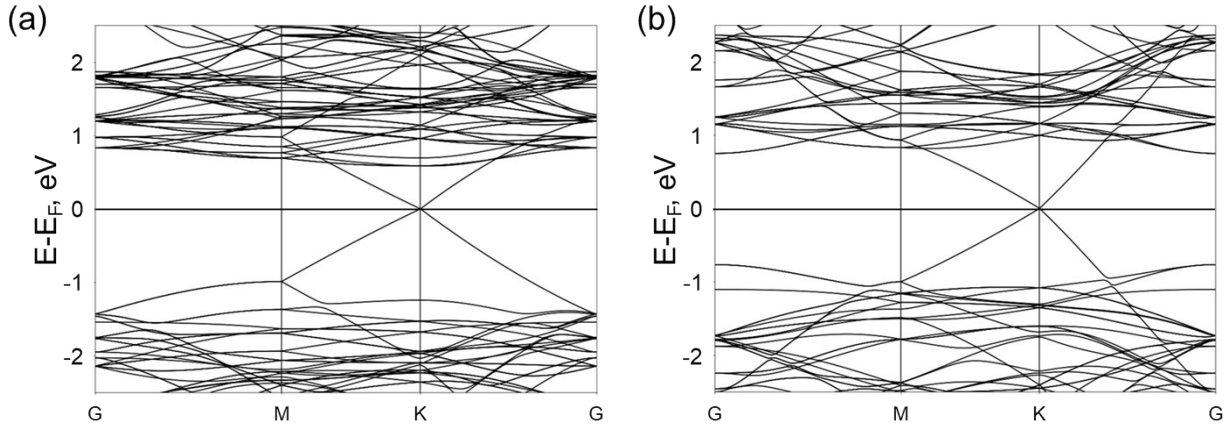

Figure S7. Electronic band structures for (a) MoS_2/graphene and (b) $MoSe_2$/graphene heterostructures.

Table S4. Minimum interlayer distances between transition metal dichalcogenide and graphene layers. The distance was found relative to chalcogen atoms and dopant atom.

Heterostructure	Dopant atom	Distance, Å	
		From S(Se) atom	From dopant atom
MoS_2/graphene	-	3.40	-
MoS_2*/graphene	F	3.28	3.50
	Cl	3.34	3.17
	Br	3.41	3.07
	I	3.43	2.92
$MoSe_2$/graphene	-	3.44	-
$MoSe_2$*/graphene	F	3.42	3.78
	Cl	3.44	3.52
	Br	3.46	3.36
	I	3.51	3.22

Table S5. Energy shift of the Dirac cone relative to the Fermi energy for the MoS_2*/graphene and $MoSe_2$*/graphene heterostructures. Positive values correspond to displacement deeper into the valence band, negative values correspond to shift deeper into the conduction band

Dopant atom	Dirac cone shift, eV	
	MoS_2*/graphene	$MoSe_2$*/graphene
F	0.01	-0.02
Cl	-0.19	-0.37
Br	-0.20	-0.37
I	-0.27	-0.38

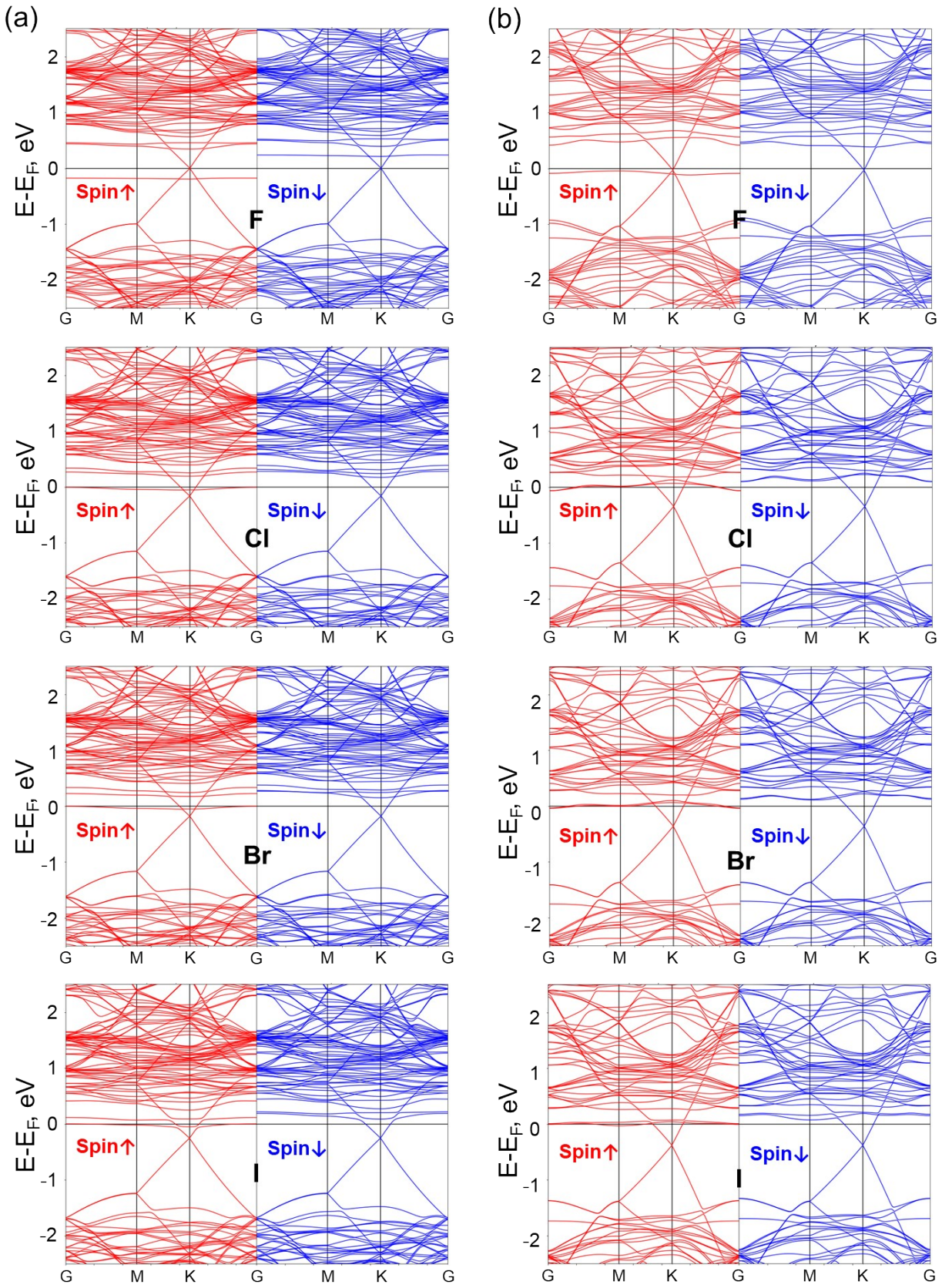

Figure S8. Spin-resolved electronic band structures for (a) MoS_2*/graphene and (b) $MoSe_2$*/graphene heterostructures.

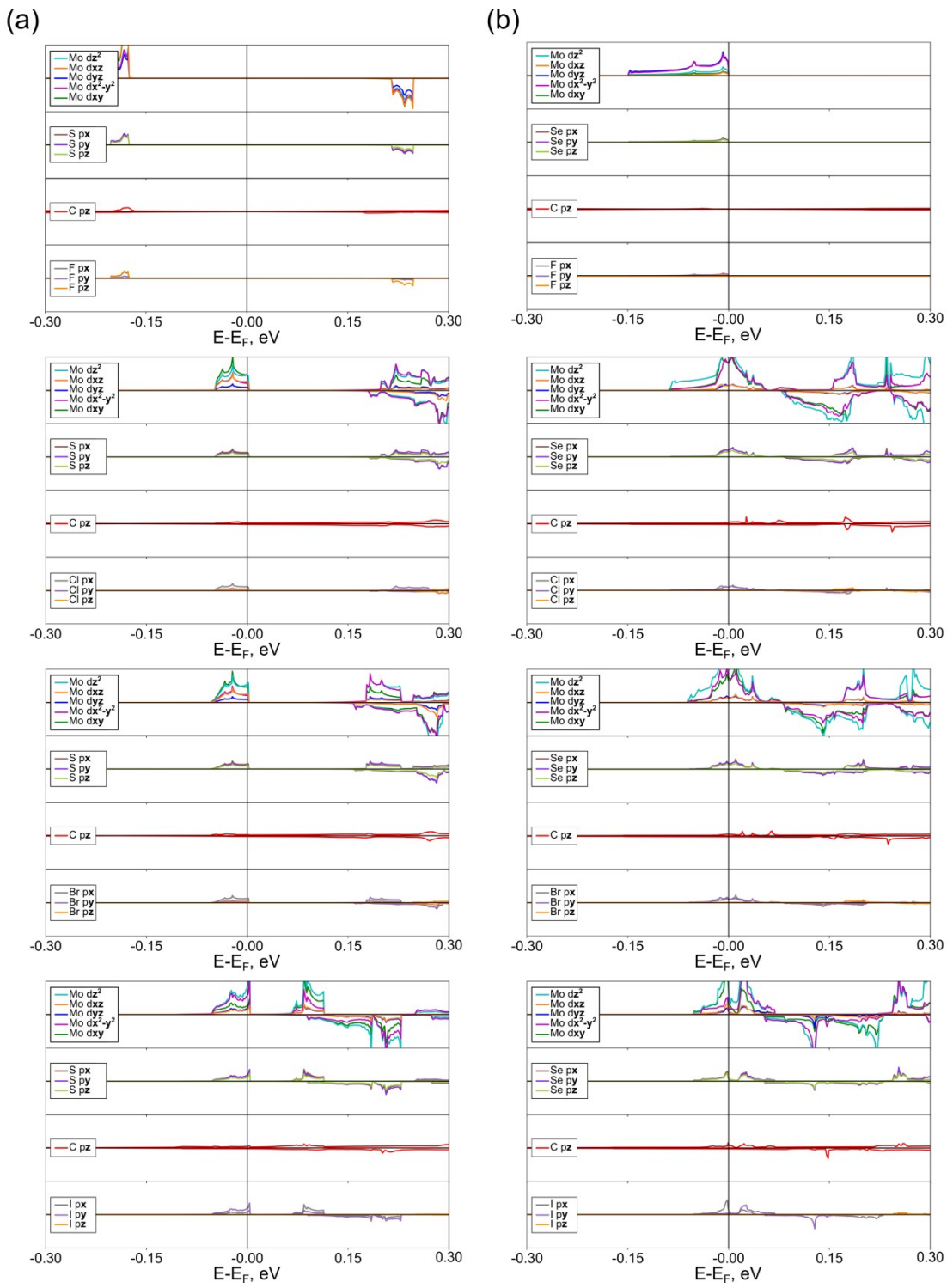

Figure S9. Orbital-resolved density of states for (a) MoS_2*/graphene and (b) $MoSe_2$*/graphene heterostructures.

Table S6. The number of electrons transferred from graphene to MX_2 layer per one carbon atom. Bader charge analysis and Charge density difference (CDD) analysis.

Dopant atom	N_e,10^{-4} per C atom			
	MoS_2*/graphene		$MoSe_2$*/graphene	
	Bader	CDD	Bader	CDD
-	8.07	20.70	-4.09	21.48
F	8.97	20.74	-3.09	19.14
Cl	0.76	13.16	-34.82	-8.85
Br	-2.25	10.70	-38.21	-10.53
I	-11.35	7.24	-43.00	-12.54

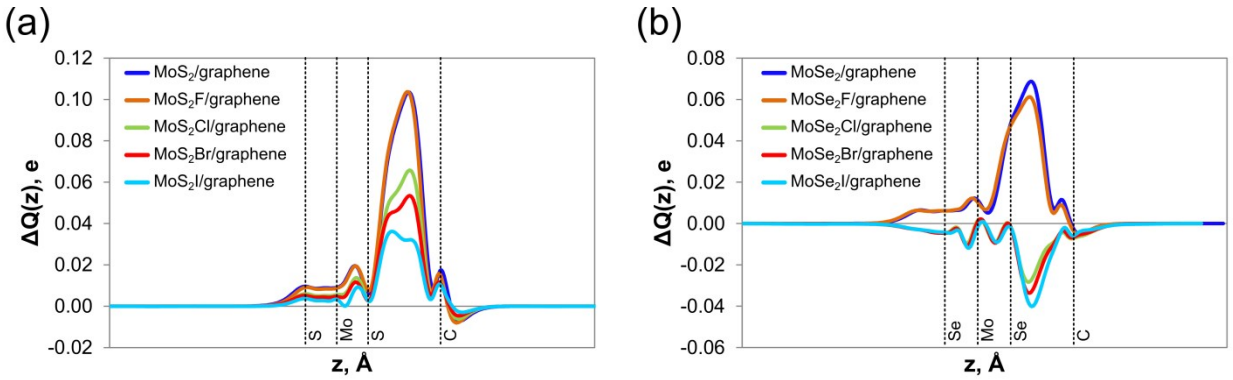

Figure S10. The amount of charge transferred from graphene to MoX_2* (X = S, Se) layer among the normal direction $\Delta Q(z)$ estimated by charge density difference analysis.

References

(1) Coehoorn, R.; Haas, C.; Dijkstra, J.; Flipse, C. J. F.; De Groot, R. A.; Wold, A. Electronic Structure of MoSe 2, MoS 2, and WSe 2. I. Band-Structure Calculations and Photoelectron Spectroscopy. *Physical review B* **1987**, *35* (12), 6195.

(2) Gupta, T. K. Preparation and Characterization of Layered Superconductors. *Physical Review B* **1991**, *43* (7), 5276.

(3) Zheng, H.; Yang, B.; Wang, D.; Han, R.; Du, X.; Yan, Y. Tuning Magnetism of Monolayer MoS2 by Doping Vacancy and Applying Strain. *Applied Physics Letters* **2014**, *104* (13), 132403.

(4) Santosh, K.; Longo, R. C.; Addou, R.; Wallace, R. M.; Cho, K. Impact of Intrinsic Atomic Defects on the Electronic Structure of MoS2 Monolayers. *Nanotechnology* **2014**, *25* (37), 375703.

(5) Cao, D.; Shu, H. B.; Wu, T. Q.; Jiang, Z. T.; Jiao, Z. W.; Cai, M. Q.; Hu, W. Y. First-Principles Study of the Origin of Magnetism Induced by Intrinsic Defects in Monolayer MoS2. *Applied Surface Science* **2016**, *361*, 199–205.

(6) Lin, Z.; Yan, H.; Liu, J.; An, Y. Defects Engineering Monolayer MoSe2 Magnetic States for 2D Spintronic Device. *Journal of Alloys and Compounds* **2019**, *774*, 160–167.

(7) Shafqat, A.; Iqbal, T.; Majid, A. A DFT Study of Intrinsic Point Defects in Monolayer MoSe2. *AIP Advances* **2017**, *7* (10), 105306.

(8) Ma, Y.; Dai, Y.; Guo, M.; Niu, C.; Lu, J.; Huang, B. Electronic and Magnetic Properties of Perfect, Vacancy-Doped, and Nonmetal Adsorbed MoSe 2, MoTe 2 and WS 2 Monolayers. *Physical Chemistry Chemical Physics* **2011**, *13* (34), 15546–15553.

(9) Haldar, S.; Vovusha, H.; Yadav, M. K.; Eriksson, O.; Sanyal, B. Systematic Study of Structural, Electronic, and Optical Properties of Atomic-Scale Defects in the Two-Dimensional Transition Metal Dichalcogenides MX2 (M =Mo, W; X = S, Se, Te). *Phys. Rev. B* **2015**, *92* (23), 235408. https://doi.org/10.1103/PhysRevB.92.235408.

(10) Zhang, H.; Fan, X.-L.; Yang, Y.; Xiao, P. Strain Engineering the Magnetic States of Vacancy-Doped Monolayer MoSe2. *Journal of Alloys and Compounds* **2015**, *635*, 307–313.